TITLE: The hypoxic ventilatory response is facilitated by the activation of Lkb1-AMPK signalling pathways downstream of the carotid bodies

RUNNING HEAD: **The Lkb1-AMPK pathway and the HVR**

Amira D. Mahmoud[1], Andrew P. Holmes[2], Sandy MacMillan[1], Oluseye A. Ogunbayo[1], Christopher N. Wyatt[5], Mark L. Dallas[4], Prem Kumar[2], Marc Foretz[3,4,5], Benoit Viollet[3,4,5], A. Mark Evans[1*]

[1]Centre for Discovery Brain Sciences, Hugh Robson Building, University of Edinburgh, Edinburgh, EH8 9XD, UK. [2]Institute of Clinical Sciences, College of Medicine and Dental Sciences, University of Birmingham, Birmingham B15 2TT, UK. [3]Department of Neuroscience, Cell Biology and Physiology, Wright State University, 3640 Colonel Glenn Hwy, Dayton, Ohio, USA, OH 45435. [4]School of Pharmacy, University of Reading, Reading RG6 6UB. [3]Institut Cochin, INSERM U1016, [4]CNRS UMR 8104 and [5]Université Paris Descartes, Sorbonne Paris cité, Paris, France.

[*]**CORRESPONDING AUTHOR**: A. Mark Evans, Discovery Brain Sciences, College of Medicine and Veterinary Medicine, Hugh Robson Building, University of Edinburgh, Edinburgh, EH8 9XD, UK. E-mail: mark.evans@ed.ac.uk

AUTHORS' CONTRIBUTIONS

A.M.E. wrote the manuscript and made Figures 3, 6 and 7. A.D.M made Figures 1, 2, 4 and 8 and supplementary Figures 1-4. S.M. made Figure 5. A.M.E. and O.A.O developed the conditional *Lkb1* knockout mice. A.M.E., A.D.M. and S.M. developed the conditional *AMPK* knockout mice, and performed genotyping. M.F. and B.V. developed the *AMPK* floxed mice. A.D.M. designed and validated primers. A.D.M. performed single cell PCR. A.M.D, S.M., and A.M.E. performed plethysmography on LKB1 and/or AMPK knockouts. A.D.M., S.M., and A.M.E. analysed respiratory data. A.P.H. and P.K. performed afferent discharge blind and under subcontract at the University of Birmingham. C.N.W. developed the murine carotid body type I cell isolation, and trained M.L.D., who carried out the type I cell isolation in support of this study.

Keywords: AMPK / apnoea / CaMKK2 / carotid body / hypoxia / LKB1 / ventilation

ABSTRACT

We recently demonstrated that the role of the AMP-activated protein kinase (**AMPK**), a ubiquitously expressed enzyme that governs cell-autonomous metabolic homeostasis, has been extended to system-level control of breathing and thus oxygen and energy (ATP) supply to the body. Here we assess the contribution to the hypoxic ventilatory response (HVR) of two upstream kinases that govern the activities of AMPK. Lkb1, which activates AMPK in response to metabolic stress and CaMKK2 which mediates the alternative Ca^{2+}-dependent mechanism of AMPK activation. HVRs remained unaffected in mice with global deletion of the CaMKK2 gene. By contrast, HVRs were markedly attenuated in mice with conditional deletion of LKB1 in catecholaminergic cells, including carotid body type I cells and brainstem respiratory networks. In these mice hypoxia evoked hypoventilation, apnoea and Cheyne-Stokes-like breathing, rather than hyperventilation. Attenuation of HVRs, albeit less severe, was also conferred in mice carrying ~90% knockdown of Lkb1 expression. Carotid body afferent input responses were retained following either ~90% knockdown of Lkb1 or AMPK deletion. In marked contrast, LKB1 deletion virtually abolished carotid body afferent discharge during normoxia, hypoxia and hypercapnia. We conclude that Lkb1 and AMPK, but not CaMKK2, facilitate HVRs at a site downstream of the carotid bodies.

1. BACKGROUND

The AMP-activated protein kinase (AMPK) is a cellular energy sensor that maintains cell-autonomous energy homeostasis. From its 2 α (catalytic), 2 β and 3 γ (regulatory) subunits 12 AMPK heterotrimers may be formed, each harbouring different sensitivities to activation by increases in cellular AMP and ADP, and the capacity to directly phosphorylate and thus regulate different targets [1]. AMPK is coupled to mitochondrial oxidative phosphorylation by two discrete albeit cooperative pathways, involving liver kinase B1 (Lkb1) and changes in the cellular AMP:ATP and ADP:ATP ratios. Binding of AMP to the AMPK γ subunit increases activity 10-fold by allosteric activation alone, while AMP or ADP binding delivers increases in Lkb1-dependent phosphorylation and reductions in dephosphorylation of Thr172 on the α subunit that confer 100-fold further activation. All of these effects are inhibited by ATP [2]. Lkb1 is, therefore, the principal pathway for AMPK activation during metabolic stresses such as hypoxia. However, there are alternative Ca^{2+}-dependent pathways to AMPK activation that are governed by the calmodulin-dependent protein kinase CaMKK2, which delivers increases in Thr172 phosphorylation and thus AMPK activation independent of changes in cellular AM(D)P:ATP ratios.

Classically AMPK regulates cell-autonomous pathways of energy supply by phosphorylating targets that switch off non-essential anabolic processes that consume ATP and switch on catabolic pathways that generate ATP, thereby compensating for deficits in ATP supply or availability[1]. Recently, however, we demonstrated [3] that the role of AMPK in metabolic homeostasis is not limited to such cell autonomous pathways, but extends to the hypoxic ventilatory response (HVR)[4, 5] and thus O_2 and energy (ATP) supply to the body as a whole. In doing so AMPK acts to oppose central respiratory depression during hypoxia and thus resists hypoventilation and

apnoea. Surprisingly, however, AMPK deficiency did not precipitate ventilatory dysfunction at the level of the carotid bodies as one would predict given their role as the primary arterial chemoreceptors [5-8], but attenuated activation during hypoxia of the caudal brainstem while afferent input responses from the carotid bodies were normal [3]. We therefore hypothesised that AMPK may aid delivery of HVRs by integrating "local hypoxic stress" within brainstem respiratory networks with an index of "peripheral hypoxic status" provided via afferent chemosensory inputs. In this respect it is clear that the capacity for signal integration could be determined centrally either through AMPK activation consequent to brainstem hypoxia, increases in the AM(D)P:ATP ratio and thus Lkb1-dependent phosphorylation, or CaMKK2-dependent phosphorylation in response to increases in cytoplasmic Ca^{2+}.

Using a variety of genetic mouse models, along with both *in vitro* and *in vivo* approaches, the present study examines whether Lkb1 and/or CaMKK2 are important drivers of HVRs. We reveal that Lkb1-AMPK signalling pathways facilitate HVRs independent of CaMKK2.

2. RESULTS

Because global gene deletion of *Lkb1* or *AMPKα1+α2* is embryonic lethal we employed conditional deletion of these genes. For *Lkb1* deletion we used floxed mice in which the gene enoding Lkb1 (*Stk11*) had been replaced by a cDNA cassette encoding equivalent exon sequences, and exon 4 and the cDNA cassette flanked by loxP sequences, which in their own right deliver ~90% global knockdown of Lkb1 expression [9]. For *AMPKα1+α2* deletion critical exons of the genes encoding AMPKα1 (*Prkaa1*) and AMPKα2 subunits (*Prkaa2*) were flanked by loxP sequences [10]. Each floxed mouse line was crossed, as previously described [3], with mice expressing Cre recombinase under the control of the tyrosine hydroxylase (TH) promoter, providing for gene deletion in all catecholaminergic cells inclusive of those cells that constitute the

hypoxia-responsive respiratory network from carotid body [8] to brainstem [11]. Transient developmental expression of TH does occur in disparate cell types that do not express TH in the adult [12], such as dorsal root ganglion cells and pancreatic islets, but these do not contribute to the acute HVR. We previously confirmed restriction of Cre to TH-positive cells in the adult mouse by viral transfection of a Cre-inducible vector carrying a reporter gene[3]. Therefore, our approach overcomes embryonic lethality and allows, unforeseen ectopic Cre expression aside, for greater discrimination of circuit mechanisms than would be provided for by global knockouts. The role of CaMKK2 in the hypoxic ventilatory response (HVR) was determined by assessing mice with global deletion of the corresponding gene (*CaMKK2*) [13].

Under normoxia there was no difference between controls and either *Lkb1*, *CaMKK2* or, as previously shown, *AMPKα1+α2* knockouts[14] with respect to weight versus age, breathing frequency, tidal volume or minute ventilation (**Supplementary Fig 1 and 2**). Nevertheless, profound and genotype-specific differences were observed with respect to the ventilatory responses during hypoxia and hypercapnia.

2.1 HVRs are attenuated in mice with Lkb1 deficiency but remain unaffected by global CaMKK2 deletion

Attenuation of HVRs was observed in *Lkb1* floxed mice used here, which harbour ~90% global Lkb1 deficiency [9]. In this respect it is notable (see below) that this effect only reached significance, compared to controls (C57/Bl6 and TH-Cre), during the sustained phase of the response to severe but not moderate hypoxia (**Fig 1A-B**), i.e. these mice exhibited delayed hypoventilation during hypoxia. This provides indirect support of our proposal that AMPK facilitates HVRs downstream of the carotid bodies, because this observation is accordance with the view that carotid body chemoafferent input responses drive the augmenting phase of HVRs [15,

16] while activation by hypoxia of brainstem respiratory networks may provide for maintenance of HVRs in the longer term [3, 5, 16-19].

The effect of conditional *Lkb1* deletion (**Fig 2, and Supplementary Fig 3**) was more severe, with HVRs suppressed, relative to controls (TH-Cre), during 5 min exposures to either mild (12% O_2; **Fig 2AI and BI *upper panels***) or severe hypoxia (8% O_2; **Fig 2AII and BII *upper panels***) and in a manner proportional to the severity of hypoxia. Relative to control mice (TH-Cre), the peak change in minute ventilation (~30s) achieved by *Lkb1* knockouts during the initial "Augmenting Phase" was lower ($P<0.0001$, compared to TH-Cre). This is important because there is general agreement that this phase of the HVR primarily results from carotid body afferent input responses [4, 5, 15]. Minute ventilation was similarly depressed relative to controls following subsequent ventilatory depression (Roll Off, ~100s, NS) and during the latter sustained phase of the response to hypoxia (2-5min; $P<0.0001$). Note: 0.05% CO_2 used here is probably insufficient to prevent significant respiratory alkalosis which may have impacted ventilatory reflexes during the latter phases of the sustained hypoxic stimulus [20] of wild type mice in particular. Therefore, we may have underestimated the degree to which *Lkb1* deletion inhibits HVRs.

By contrast, global deletion of CaMKK2 did not affect HVRs in any discernable way (**Fig 2BI-II *lower panels***), ruling out a prominent role for AMPK activation through this alternative Ca^{2+}-dependent pathway.

2.2 Attenuation of HVRs by *Lkb1* deletion results from deficits in breathing frequency

Intriguingly, deficits in minute ventilation in *Lkb1* floxed mice resulted from attenuation of increases in breathing frequency at all time points during exposure to severe (8% O_2; n=22; $P\leq0.0001$) but not mild (12%; n=15; NS) hypoxia. Increases in breathing frequency were even more markedly attenuated by homozygous *Lkb1* deletion and at all time points during exposure to both mild and severe hypoxia when compared to controls (TH-Cre; $P<0.0001$; **Fig 3A**), albeit in a

manner proportional to the severity of hypoxia. By contrast no attenuation of increases in tidal volume were observed for either *Lkb1* floxed mice or *Lkb1* knockouts during mild or severe hypoxia.

The aforementioned findings are intriguing because it has been proposed that peripheral chemoreceptors primarily drive increases in breathing frequency during moderate to severe hypoxia (see for example [21]). It is therefore all the more important to note that mice with conditional deletion of *AMPKα1+α2* in catecholaminergic cells, which retain carotid body afferent input responses, exhibit markedly attenuated increases in breathing frequency but not tidal volume at all time points when exposed to mild hypoxia (12% O_2; **Fig 3A-B**). By contrast, however, *AMPKα1+α2* deletion attenuated increases in both breathing frequency and tidal volume during severe (8% O_2) hypoxia [14]. When taken together these findings strongly suggest that Lkb1-AMPK signalling pathways facilitate HVRs and oppose respiratory depression during hypoxia. Moreover, outcomes suggest that those circuit mechanisms that mediate hypoxia-evoked increases in tidal volume are afforded greater protection from the impact of Lkb1 and AMPK deficiency than those delivering increases in breathing frequency.

2.3 Lkb1 deficiency causes ventilatory instability and Cheyne-Stokes-like breathing during hypoxia.

Quite unlike our previously reported findings in mice with *AMPKα1+α2* deletion[14], average measures (excluding apnoeas) for *Lkb1* knockouts indicated significant augmentation rather than attenuation of increases in tidal volume during severe hypoxia, relative to controls ($P<0.01$ at 100s and 300s compared to TH-Cre). Closer inspection revealed that attenuation of HVRs in *Lkb1* knockouts during exposure to 8% O_2 only, was associated with periods of Cheyne-Stokes-like breathing (CSB), i.e., tidal volume exhibited marked, sinusoidal variations with time (**Fig 4A and B**). Periods of CSB in *Lkb1* knockout mice were generally separated by frequent, prolonged

apnoeas (≤4s), with apnoea frequency, apnoea duration and apnoea duration index (frequency x duration) all significantly larger (P<0.0001) than for controls (**Fig 4C**). Nevertheless, as might be expected given outcomes for minute ventilation, apnoea frequency and duration also increased in a manner directly related to the severity of hypoxia. Moreover, CSB and increases in apneoa frequency and duration observed during severe hypoxia were completely reversed by hypercapnic hypoxia (**Fig 4AIII and C**), likely due to improved O_2 supply consequent to increases in ventilation (see below). The appearance of CSB likely accounts for measured increases in tidal volume for these mice relative to controls. That aside it is important to note that periods of hypoxia-evoked CSB in *Lkb1* knockouts occurred irrespective of whether they were preceded by spontaneous or post-sigh apnoeas (**Fig 4B**). Moreover both spontaneous and post-sigh apnoeas were equally frequent during exposure of *AMPKα1+α2* knockouts to severe hypoxia, where CSB is absent during 5 min [3] or even 10 min (**Fig 5**) exposures to severe hypoxia. In short, if sighs are triggered by hypoxia at a given threshold [3, 22], central hypoxia is likely no more severe for *Lkb1* when compared to *AMPKα1+α2* knockouts and CSB consequent to Lkb1 deficiency is thus most likely triggered by other means.

2.2 Conditional *Lkb1* deletion slows the ventilatory response to hypercapnic hypoxia and hypercapnia

The ventilatory response to hypercapnic hypoxia (8% O_2 + 5% CO_2) remained entirely unaffected following *AMPKα1+α2* deletion [3]. By contrast, in *Lkb1* knockouts increases in minute ventilation were attenuated, but only during the rising phase of the ventilatory response to hypercapnic hypoxia (P<0.01; **Fig 6A**), indicating that *Lkb1* deletion slowed the rising phase of the response to this stimulus but did not affect the peak achieved. It is possible that this may reflect the partial restoration of the initial rise in respiratory frequency during hypercapnic hypoxia, that is

197 attenuated during hypoxia alone (**Supplementary Fig 4**). However, the rise in minute ventilation
198 during exposure to hypercapnia alone (5% CO_2) was also markedly slower for *Lkb1* knockouts
199 ($P<0.05$), but thereafter achieved an equivalent magnitude (**Fig 6B**), as a consequence of equivalent
200 peak increases in both respiratory frequency and tidal volume **(Supplementary Fig 4**). By contrast,
201 mice with *AMPKα1+α2* deletion had preserved peak hypercapnic ventilatory responses without
202 any initial delay in onset (**Fig 6A-B**).
203
204 **2.3 *Lkb1* but not *AMPKα1+α2* deletion attenuates carotid body chemoafferent discharge**
205 **during normoxia, hypoxia and hypercapnia**
206 During normoxia mean±SEM basal afferent fibre discharge frequency from *in-vitro* carotid bodies
207 of TH-Cre mice was similar to that for carotid bodies of homozygous *Lkb1* floxed mice that harbour
208 ~90% global Lkb1 deficiency [9]. In marked contrast, however, basal afferent discharge measured
209 from carotid bodies of *Lkb1* knockouts was markedly attenuated (**Fig 7C**; n=7; $P\leq0.001$ versus
210 TH-Cre and *Lkb1* floxed).
211 In line with the above, reductions in superfusate PO_2 increased chemoafferent discharge from
212 carotid bodies of TH-Cre mice exponentially, but evoked only marginal increases in afferent
213 discharge from carotid bodies of *Lkb1* knockouts ($P<0.0001$; **Fig 7C**). By contrast, peak discharge
214 frequencies (PO_2 ≤75 mmHg) of carotid bodies from hypomorphic *Lkb1* floxed mice were
215 attenuated by less than 50% relative to controls, despite the fact that these mice exhibit global
216 deficits in Lkb1 expression of ~90% [9]
217 For *AMPKα1+α2* deletion basal afferent discharge frequency was higher than recorded for
218 *AMPKα1+α2* floxed mice (n=5; $P<0.001$) [3], but not significantly different from measures for
219 either TH-Cre (n = 8) or the hypomorphic *Lkb1* floxed (n =7) mice. *AMPKα1+α2* floxed mice may
220 represent the better comparison, raising the possibility that AMPK may ordinarily act to reduce

basal afferent discharge frequency through, for example, inhibition of the large conductance voltage- and calcium-activated potassium current (BK_{Ca})[23]. However, it is clear that this does not hold when basal discharge of *AMPKα1+α2* knockouts is compared against our full range of control mice. Moreover, peak discharge frequency during hypoxia (**Fig 7C**) was similar for *AMPKα1+α2* knockouts when compared to *AMPKα1+α2* floxed (n=5; NS) and TH-Cre mice (n=8; NS).

Carotid bodies isolated from *AMPKα1+α2* knockouts also had a preserved chemoafferent response to hypercapnia. By contrast, *Lkb1* deletion (n=4) inhibited carotid body responses to hypercapnia and reduced carotid body CO_2-sensitivity (which is linear between 40 and 80 mmHg) when compared to TH-Cre (n=7; **Fig 7D**). This may explain, in part, the slower rising phase of the ventilatory response of *Lkb1* knockouts during hypercapnic hypoxia and hypercapnia, as carotid body afferent inputs to the brainstem determine this [15, 24].

2.4 The rank order of severity for HVR versus carotid body dysfunction is different

As demonstrated above, while *Lkb1* deletion virtually abolished, hypomorphic Lkb1 expression modestly attenuated and *AMPKα1+α2* deletion was without effect on afferent output from the carotid body during hypoxia, all three interventions markedly attenuated the HVR during severe hypoxia. Moreover, the order of severity for hypoxic ventilatory dysfunction was different when compared to that for inhibition of carotid body chemoafferent discharge during hypoxia. This is evident from **Fig 8,** which compares Poincaré plots of inter-breath interval (BBn) versus subsequent inter-breath interval (BBn+1) during normoxia (**AI**), 12% O_2 (**BI**), 8% O_2 (**CI**), 8% O_2 + 5% CO_2 (**DI**) for controls (TH-Cre), hypomorphic *Lkb1* floxed mice and *Lkb1* knockouts (**Fig 8AI-DI**, *left hand panels*) with previously published [3] examples for *AMPKα1+α2* knockouts (**Fig 8AI-DI**, *right hand panels*)**,** the SD of inter-breath intervals (**Fig 8AII-DII**), minute ventilation (**Fig 8E**), and apnoea frequency, duration and duration index (**Fig 8F I-III**). Clearly, ventilatory

dysfunction worsened with progressive loss of Lkb1, but was most severe following *AMPKα1+α2* deletion.

3. DISCUSSION

The present study demonstrates that deletion of *Lkb1* or *AMPKα1+α2*, but not *CaMKK2*, attenuates HVRs, precipitating hypoventilation and apnoea during hypoxia. The LKB1-AMPK signalling pathway is therefore critical to the delivery of ventilatory drive during hypoxia, and acts to oppose ventilatory depression, hypoventilation and apnoea. However, surprising differences between *Lkb1* and *AMPKα1+α2* knockouts were identified with respect to both HVRs and carotid body afferent fibre discharge, which provides further substantiation of our proposal [3] that AMPK facilitates HVRs downstream of peripheral chemoafferent input responses, most likely at the brainstem.

Of particular note in this respect was the fact that LKB1 deletion attenuated HVRs and hypoxia-evoked increases in carotid body afferent discharge, while by contrast *AMPKα1+α2* deletion abolished HVRs but had little if any effect on carotid body afferent discharge during hypoxia [3]. Irrespective of the precise cellular mechanism, it is therefore clear that we have uncovered a split in the dependency on Lkb1 and AMPK of carotid body chemoafferent discharge during hypoxia on the one hand and HVRs on the other.

This view gained support from our studies on *Lkb1* floxed mice, which exhibit ~90% global Lkb1 deficiency [9], but retain significantly greater capacity for basal and hypoxia-evoked carotid body afferent discharge than do *Lkb1* knockouts and yet still exhibit delayed hypoventilation and apnoea during severe hypoxia (8% O_2). Intriguingly in this respect, deficits in minute ventilation were evident for *Lkb1* floxed mice during the sustained but not the augmenting phase. This is entirely consistent with an inhibitory effect downstream of chemoafferent input responses, if one accepts evidence supporting the view that increases in carotid body afferent discharge drive the augmenting phase of HVRs [15, 16] while direct modulation by hypoxia of brainstem respiratory networks

maintains HVRs in the longer term [3-5, 16, 17]. Further support for this proposal may be derived from the fact that the order of severity for hypoxic ventilatory dysfunction increases progressively with the degree of Lkb1 deficiency (Fig. 5), but is most severe following *AMPK-α1+α2* deletion [3]. This is in spite of our finding that only *Lkb1* deletion attenuates carotid body afferent discharge, and suggests that the increased severity of ventilatory instability during sustained hypoxia is governed centrally by AMPK activity in catecholaminergic neurons.

Differences in outcome between genotypes provide yet further insights into the underlying circuit mechanisms governing HVRs. Hypomorphic *Lkb1* floxed mice exhibit marked attenuation of breathing frequency responses during severe hypoxia while tidal volume responses remained largely unaltered. AMPKα1/α2 deletion similarly attenuated only breathing frequency during mild hypoxia (12% O_2), but blocked increases in both breathing frequency and tidal volume during severe hypoxia. Given that HVRs of mice hypomorphic for Lkb1 are less severely compromised than that of mice following *AMPKα1+α2* deletion, these outcomes suggest that the PO_2-dependence for depression of breathing frequency is steeper than that for tidal volume in mice with deficiencies within the Lkb1-AMPK signalling pathway. AMPK may therefore contribute to each component of HVRs via divergent brainstem networks that lie downstream of carotid body afferent input responses, a point emphasised by the fact that *AMPKα1+α2* deletion is without effect on carotid body afferent discharge during hypoxia. That this may be the case gains further support from the generally held view that increases in breathing frequency during moderate to severe hypoxia are primarily driven by carotid body afferent input responses (see for example [21]).

Consistent with the aforementioned proposals, homozygous *Lkb1* deletion led to marked reductions in breathing frequency (excluding apnoeas) that were coupled with erratic "augmentation" of tidal volume responses during severe hypoxia. An explanation for this apparent increase in tidal volume was provided by the fact that *Lkb1* knockouts exhibited pronounced Cheyne-Stokes-like breathing

(CSB) during hypoxia. That said, it is curious to note that CSB in *Lkb1* knockouts is accompanied by loss of carotid body afferent inputs given that hyperactivity of these peripheral chemoreceptors has been identified as the cause of CSB when associated with heart failure [25]. One possible explanation for this contrary outcome could be that *Lkb1* deletion alone attenuated basal afferent discharge from the carotid body and virtually abolished increases in chemoafferent discharge during hypoxia and hypercapnia, actions that could serve to attenuate any inhibitory interactions between peripheral chemoreceptors and brainstem respiratory networks [15, 24]. That this might be the case is indicated by the fact that the peak of the sustained phase of the hypercapnic ventilatory response of *Lkb1* knockouts remained unaltered despite the reduction of afferent input responses. In other words, increases in controller gain within the central respiratory network could trigger CSB by enhancing the sensitivity to, and thus the degree of activation of central CO_2-sensing neurons during hypercapnia [15] consequent to hypoventilation during hypoxia, leading to periodic augmentation of tidal volume in *Lkb1* knockouts alone. Consistent with this view, others have proposed that CSB may be caused by enhanced hypercapnic ventilatory responses driven by instability within respiratory networks consequent to either augmented chemoreflex gain, prolonged feedback delay [26] and/or enhanced central controller gain [27]. In short, apnoeic intervals may well be countered earlier in *Lkb1* knockouts through augmented central hypercapnic ventilatory responses consequent to reductions in basal and evoked carotid body afferent discharge frequencies [15, 24], resulting in CSB during periods of hypoxia-evoked reductions in breathing frequency. The more extreme patterns of non-rhythmic (ataxic) ventilation observed for *AMPKα1/α2* knockouts [3] may thus be avoided. While less likely it is also conceivable that retention by *Lkb1* knockouts of greater capacity for rhythmic ventilation during hypoxia could be conferred by residual allosteric AMPK activation by AMP, because this occurs independent of Lkb1 [1] and any fall in cellular ATP supply during hypoxia would be associated with not only

317 ADP accumulation but consequent increases in the AMP:ATP ratio via the adenylate kinase
318 reaction. This may in its own right be sufficient to maintain oscillating central respiratory drive in
319 a manner periodically triggered once a given severity of central hypoxia is breached. That said, if
320 sighs are triggered by hypoxia at a given threshold [22, 28], central hypoxia is likely no more severe
321 for *Lkb1* when compared to *AMPKα1+α2* knockouts because: (1) A similar frequency of sighs is
322 observed during hypoxia for each of these genotypes; (2) Apnoeas are shorter and less frequent for
323 *Lkb1* when compared to *AMPKα1+α2* knockouts; (3) Only *Lkb1* knockouts exhibit CSB between
324 apnoeas, which would periodically raise O_2 supply. Therefore, unless loss of carotid body afferent
325 input responses in *Lkb1* knockouts alters functional hyperaemia at the level of the brainstem and
326 via neuronal pathways independent of those mediating HVRs, it seems most likely that differences
327 in outcome between genotypes arise from means other than variations in severity of brainstem
328 hypoxia. However, for this question to be answered conclusively we would need to identify the
329 precise hypoxia-responsive brainstem region(s) affected by our gene deletion strategies and obtain
330 direct, region-specific measurements of local PO_2.
331 While the aforementioned findings run counter to the view that increased afferent discharge from
332 carotid body to brainstem alone determines the ventilatory response to a fall in arterial PO_2 they
333 do provide substantial support for an alternative yet inclusive perspective, namely that HVRs are
334 determined by the coordinated action of the carotid body and an hypoxia-responsive circuit within
335 the brainstem [3, 5, 16, 17]. To date little emphasis has been placed on the role of hypoxia-sensing
336 downstream, at the level of the brainstem perhaps because HVRs are so effectively abolished by
337 resection of the carotid sinus nerve in humans [29]. And yet brainstem hypoxia induces an HVR
338 when in receipt of normoxic carotid body afferent inputs [17], and directly activates subsets of
339 catecholaminergic neurons within the brainstem nucleus of the solitary tract [30] and rostral
340 ventrolateral medulla [5, 31, 32] in a manner that may be supported by direct activation by hypoxia

of ATP/lactate release from brainstem astrocytes [33, 34]. Moreover and consistent with the fact that our gene deletion strategy targeted catecholaminergic neurons, ectopic expression aside, extensive investigations have demonstrated that following carotid body resection, hypoxia-responsive catecholaminergic neurons of the caudal brainstem may underpin partial recovery of the HVR in a variety of animal models [5]. Accordingly, dysfunction of these neurons has been shown to underpin hypoventilation and apnoea associated with Rett syndrome, which is exacerbated during hypoxia [35].

Insights into the mechanisms that determine afferent discharge from the carotid body may also be garnered from our observation that *Lkb1* but not *AMPKα1+α2* deletion markedly attenuated basal afferent fibre discharge and blocked increases in afferent discharge during hypercapnia, given that increases in afferent discharge during hypercapnia are triggered by membrane depolarisation consequent to hypercapnic acidosis and in a manner not directly influenced by reductions in mitochondrial oxidative phosphorylation or deficits in ATP supply [36]. This suggests that while *Lkb1* contributes to the maintenance of carotid body afferent discharge, it does not necessarily support type I cell oxygen-sensing *per se*. We must, however, add a note of caution here, because this assay does not directly distinguish between actions on the type I cells and tyrosine hydroxylase expressing glossopharyngeal nerves. Nevertheless, we can conclude that Lkb1 expression is somehow necessary for chemoafferent outflow from the carotid body. That said, the reduced hypercapnic chemoafferent responses could alternatively be due to the removal of CO_2-O_2 stimulus interaction [37, 38]. Either way, our findings suggest that Lkb1 determines, independent of AMPK, carotid body chemoafferent discharge [39]. Lkb1 could conceivable contribute to developmental expansion of carotid body type I cells, or to the regulation of glucose homeostasis [40, 41] and mitochondrial function [42, 43], either directly or in a manner supported by constitutive phosphorylation of one or more of the 12 AMPK-related kinases [44]. In short, a role for Lkb1 in

365 the carotid body that is independent of the modification in AMPK activity is intriguing, but further,
366 extensive investigations will be required to determine the precise mechanism(s) involved.
367
368 **4. CONCLUSION**
369 Lkb1 and AMPK provide hierarchical control of the chemo-sensory respiratory network. Firstly,
370 Lkb1 appears to determine, independent of AMPK, a set-point about which carotid body afferent
371 input responses are evoked during hypoxia and hypercapnia, rather than contributing to oxygen-
372 sensing *per se*. Thereafter the Lkb1-AMPK signalling pathway likely governs, through the capacity
373 for AMPK activation by increases in AM(D)P/ATP ratio and Lkb1-dependent phosphorylation,
374 coincidence detection and thus signal integration within a hypoxia-responsive circuit downstream
375 of the carotid body, that encompasses, at the very least, the nucleus of the solitary tract and
376 ventrolateral medulla [3]. Afferent input responses and brainstem hypoxia could thereby determine,
377 each in part, the set-point about which AMPK and thus the brainstem respiratory networks are
378 activated during hypoxia. Subsequently, AMPK-dependent modulation of cellular metabolism[1],
379 ion channels [23, 45] and thus neuronal activities [46, 47] may facilitate efferent output and
380 increases in ventilatory drive during hypoxia. It is therefore conceivable that Lkb1 and/or AMPK
381 deficiency may contribute to Cheyne-Stokes breathing [26] and/or sleep disordered breathing
382 associated with, for example, heart failure [25], metabolic syndrome-related disorders[48] and
383 ascent to altitude [49].
384
385 **5. METHODS**
386 Experiments were carried out as described previously[3], were approved by local ethical review
387 committees, the University Director of Veterinary Services and the Home Office (Science, UK),

and complied with the regulations of the United Kingdom Animals (Scientific Procedures) Act of 1986.

5.1 Breeding of mice, genotyping and single cell PCR

Standard approaches were used. All mice studied were between 3-12 months of age. Both males and females were studied.

For *Lkb1* deletion we used mice with exons 5-7 of the *Lkb1* gene (STK11) replaced by a cDNA cassette encoding equivalent exon sequences, and exon 4 and the cDNA cassette flanked by loxP sequences ($Lkb1^{fl/fl}$). These mice were crossed with transgenic mice expressing Cre-recombinase under the tyrosine hydroxylase promoter (Th-IRES-Cre; EM:00254)[12]. Wild type or floxed *Lkb1* alleles were detected using two primers, p200, 5'-CCAGCCTTCTGACTCTCAGG-3' and p201, 5'-GTAGGTATTCCAGGCCGTCA-3'. For the detection of CRE recombinase we employed: TH3, 5'-CTTTCCTTCCTTTATTGAGAT-3', TH5, 5'-CACCCTGACCCAAGCACT-3' and Cre-UD, 5'-GATACCTGGCCTGGTCTCG-3'. As $Lkb1^{fl/fl}$ mice are hypomorphic, exhibiting 5-10 fold lower LKB1 expression than $Lkb1^{+/+}$ littermates [9], we used as controls mice that express Cre via the tyrosine hydroxylase promoter (TH-Cre).

For deletion of the gene that encodes CaMKK2 (*CaMKK2*) wild type alleles were detected using two primers, KKBeta1, 5'CAGCACTCAGCTCCAATCAA3', and KKBeta2, 5'GCCACCTATTGCC TTGTTTG3'. The PCR protocol used for all genotype primers was: 92ºC for 5min, 92ºC for 45s, 56ºC for 45s, 72ºC for 60s, and 72ºC for 7min for 35 cycles and then 4ºC as the holding temperature. 15 µl samples were run on 2% agarose gels with 10 µl SYBR®Safe DNA Gel Stain (Invitrogen) in TBE buffer against a 100 bp DNA ladder (GeneRuler™, Fermentas) using a Model 200/2.0 Power Supply (Bio-Rad). Gels were imaged using a Genius Bio Imaging System and GeneSnap software (Syngene).

We also used conditional deletion of the genes for the *AMPKα1* and *α2* subunits, utilising mice in which the sequence encoding the catalytic site of both of the α subunits was flanked by loxP sequences (*α1^{flx} and α2^{flx}* [10]). We used two primers for each AMPK catalytic subunit: α1-forward: 5' TATTGCTGCCATTAGGCTAC 3', α1-reverse: 5' GACCTGACAGAATAGGATATGCCCAACCTC 3'; α2-forward 5' GCTTAGCACGTTACCCTGGATGG 3', α2-reverse: 5' GTTATCAGCCCAACTAATTACAC 3'. To direct *AMPK* deletion to identified oxygen-sensing cells of the carotid body and brainstem, these were crossed with TH-Cre mice as above. We detected the presence of wild-type or floxed *AMPK* alleles *and* Cre-recombinase by PCR. 15 µl samples were run on 2% agarose gels and imaged as described above.

5.2 Single-cell end-point PCR

Carotid bodies were incubated at 37°C for 25-30 min in isolation medium consisting of: 0.125mg/ml Trypsin (Sigma), 2.5mg/ml collagenase Type 1 (Worthington) made up in low Ca^{2+}/low Mg^{2+} HBSS. During this incubation the carotid bodies were separated from the associated patch of artery. The carotid bodies were then transferred to low Ca^{2+}/low Mg^{2+} HBSS containing trypsin inhibitor (0.5mg/ml) for 5min at room temperature, and then to 2ml of pre-equilibrated (95% air, 5% CO_2, 37°C) growth medium (F-12 Ham nutrient mix, 10% fetal bovine serum, 1% penicillin/streptomycin). The medium containing the carotid bodies was centrifuged and the pellet re-suspended in 100µl of growth medium. Carotid bodies were then disrupted by triturating using fire polished Pasteur pipettes.

RNA was extracted using the High Pure RNA Tissue Kit (Roche) following the manufacturer's guidelines and the concentration determined using the Nanodrop 1000 spectrophotometer (ThermoScientific). cDNA synthesis was carried out using the Transcriptor High Fidelity cDNA synthesis Kit (Roche) following the manufacturers' instructions. Amplification of cDNA isolated

435 from different individual cells was run in parallel with negative and positive controls using an
436 initial denaturing step at 94°C for 5min and then denaturing at 94°C for 30s, annealing at 60°C for
437 45s, and extension for 60s at 72°C with a final 7min extension at 72°C. Initially 15 cycles were
438 performed, followed by reaction and dilution for a further 38 cycles. To detect tyrosine
439 hydroxylase, primers obtained from Qiagen (Quantitect Primer Assay, QT00101962) were used
440 with an expected band length of 96bp. For the detection of Lkb1 two primers were used, *forward*
441 and *reverse*, to generate an expected band length of 92bp.
442 Negative controls included control cell aspirants, lacking reverse transcriptase, aspiration of
443 extracellular medium and PCR controls; these produced no detectable amplicons, ruling out
444 genomic or other contamination. 15µl samples and a 100bp DNA ladder (GeneRuler™, Fermentas)
445 were run on 2% agarose gels with SYBR®Safe DNA Gel Stain (Invitrogen). Gels were imaged
446 using a Genius Bio Imaging System and GeneSnap software (Syngene). Positive controls were
447 from samples rich in adrenomedullary chromaffin cells, dissected from adrenal glands of C57/Bl6
448 mice. RNA was extracted using the High Pure RNA Tissue Kit (Roche) following the
449 manufacturer's guidelines and the concentration determined using the Nanodrop 1000
450 spectrophotometer (ThermoScientific). cDNA synthesis was carried out using the Transcriptor
451 High Fidelity cDNA kit (Roche) following manufacturers instructions.

452 **5.3 Quantitative RT-PCR**

453 RNA from adrenal glands was extracted, quantified and reverse transcribed as described above.
454 For qPCR analysis, 2.5 µl of cDNA in RNase free water was made up to 25 µl with FastStart
455 Universal SYBR Green Master (ROX, 12.5 µl, Roche), Ultra Pure Water (8 µl, SIGMA) and
456 forward and reverse primers for Lkb1. The sample was then centrifuged and 25 µl added to a
457 MicroAmp™ Fast Optical 96-Well Reaction Plate (Greiner bio-one), the reaction plate sealed with

an optical adhesive cover (Applied Biosystems) and the plate centrifuged. The reaction was then run on a sequence detection system (Applied Biosystems) using AmpliTaq Fast DNA Polymerase, with a 2min initial step at 50ºC, followed by a 10min step at 95ºC, then a 15s step at 95ºC which was repeated 40 times. Then a dissociation stage with a 15s step at 95ºC followed by a 20s at 60ºC and a 15s step at 95ºC. Negative controls included control cell aspirants for which no reverse transcriptase was added, and aspiration of extracellular medium and PCR controls. None of the controls produced any detectable amplicon, ruling out genomic or other contamination.

5.4 Plethysmography

We used unrestrained whole-body plethysmography, incorporating a Halcyon^{TM} low noise pneumatochograph coupled to FinePointe acquisition and analysis software with a sampling frequency of 1kHz (Buxco Research Systems, UK). All quoted values for HVR were derived from apnoea-free periods of ventilation. Any unreliable and erratic respiratory waveforms recorded during gross un-ventilatory related body movements, i.e. sniffing and grooming, were avoided for measurements. Additionally, a rejection algorithm that was built into the plethysmography system (Buxco Electronics Inc.) identified periods of motion-induced-artefacts for omission. The patented Halycon^{TM} low noise pneumotachograph (Buxco Electronics Inc.) reduces disturbances caused by air currents from outside the chambers (i.e. fans, closing doors, air conditioners, etc.), which can disrupt or overwhelm the ventilatory airflows within the chamber.

Mice were placed in the plethysmography chamber for a 10-20 min acclimation period under normoxia (room air) to establish a period of quiet and reliable breathing for baseline-ventilation levels (this is also indicated by a measured rejection index of 0 by the FinePointe Acquisition and Analysis Software). Mice were then exposed to hypoxia (12% or 8% O_2, with 0.05% CO_2, balanced with N_2), hypoxia+hypercapnia (8% O_2, 5% CO_2, balanced with N_2) or hypercapnia (21% O_2, 5% CO_2, balanced with N_2) for 5min. Medical grade gas mixtures were chosen by switching a gas tap.

The time for evacuation of the dead space and complete exchange of gas within the plethysmography chamber was 30s. The duration of exposure to hypoxia quoted was the actual duration of hypoxia. Apnoea was defined as cessations of breathing greater than the average duration, including interval, of 2 successive breaths (600ms) during normoxia, with a detection threshold of 0.25 mmHg (SD of noise). Breathing variability was assessed by Poincaré plots and by calculating the SD of inter-breath (BB) intervals. The breathing frequency, tidal volume, and minute ventilation as derived by the FinePointe Software were also analysed for control and knockout mice. These parameters were measured as mean values taken over a 2s breathing period and not on a breath-to-breath basis. The changes in breathing frequency, tidal volume, and minute ventilation during hypoxia and/or hypercapnia were analysed as the percentage change from normoxia respective to each individual mouse. The peak of the augmenting phase (A) was calculated from the peak value between 20-40s of the hypoxic and/or hypercapnic exposure that coincides with the peak of the rising phase. The roll off period was calculated as the lowest value between 60-140s of exposure and the sustained phase was calculated from the last 20s in the plateaued phase. A large time range was required for selection of these points as experiments were performed on unrestrained and awake animals and periods of no movement, sniffing, or grooming, were only considered.

Apnoeas were excluded from all stated measures (mean±SEM) of breathing frequency, tidal volume and minute ventilation, i.e., all quoted values were derived from apnoea-free periods of ventilation.

5.5 Isolated carotid body

Methods for single fibre chemoafferent activity were adapted from those described previously[14, 50]. Plots of firing frequency versus superfusate pO_2 were fitted by non-linear regression

(GraphPad Prism 6).

Single fibre chemoafferent activity was amplified and filtered and recorded using a 1401 interface running Spike 2 software (Cambridge Electronic Design). Single- or few-fibre chemoafferent recordings were made from carotid bifurcations held in a small volume tissue bath, and superfused (36-37°C) with gassed (95% O_2 and 5% CO_2), bicarbonate-buffered saline solution (composition (mM): 125 NaCl, 3 KCl, 1.25 NaH_2PO_4, 5 Na_2SO_4, 1.3 $MgSO_4$, 24 $NaHCO_3$, 2.4 $CaCl_2$). A standard O_2 electrode (ISO2; World Precision Instruments) was placed in the superfusate system at the point of entry to the recording chamber in order to continuously record the superfusate PO_2. Flow meters with high precision valves (Cole Palmer Instruments) were used to equilibrate the superfusate with a desired gas mixture. Basal single fibre activity was monitored at a superfusate PO_2 of 200mmHg and a PCO_2 of 40mmHg. This PO_2 is slightly lower than that previously used for the rat carotid body[51] to take in account the smaller size of this organ in the mouse (and thus a smaller diffusion distance). At this superfusate PO_2, the basal frequency in TH-Cre single fibres (Figure 1) was consistent with that reported *in vivo* in other rodents[52] and so we interpret this PO_2 to have not been excessively hyperoxic.

To induce responses to hypoxia, the superfusate PO_2 was slowly reduced to a minimum of 40 mmHg or was reversed prior to this when the chemoafferent response had stabilised or had begun to diminish. The single fibre chemoafferent discharge frequency was plotted against the superfusate PO_2 over a desired range of superfusate PO_2 values. To produce the hypoxic response curves, the data points were fitted to an exponential decay curve with offset, as shown below:

$$y = a + be^{-cx}$$

For the above equation, y is the single fibre discharge frequency in Hz, x is the superfusate PO_2 in mmHg, a is the discharge frequency as the PO_2 tends to infinity (offset), b is the discharge frequency when the PO_2 is 0 mmHg (minus the offset) and c is the exponential rate constant.

5.6 Statistical analysis

Statistical comparison was completed using GraphPad Prism 6 for the following: *Afferent discharge*, single or 2 factor ANOVA with Bonferroni Dunn post hoc analysis; *Plethysmography*, one-way ANOVA with Bonferroni multiple comparison's test; $P<0.05$ was considered significant.

COMPETING INTERESTS: The authors declare no competing financial interests nor any competing non-financial interests.

ACKNOWLEDGEMENTS

This work was primarily funded by the Wellcome Trust (WT081195MA). A.M.E. thanks Professor D. Grahame Hardie for his continued guidance, support and for providing the Lkb1 floxed mice. We would also like to thank Professor Michael J. Shipston and Helene Widmer for their kind help and assistance with the single cell PCR shown in the supplementary information.

REFERENCES

1. Ross F.A., MacKintosh C. & Hardie D.G. AMP-activated protein kinase: a cellular energy sensor that comes in 12 flavours. *FEBS J.* **83**, 2987-3001 (2016).
2. Gowans G.J., Hawley S.A., Ross F.A. & Hardie D.G. AMP is a true physiological regulator of AMP-activated protein kinase by both allosteric activation and enhancing net phosphorylation. *Cell Metab.* **18**, 556-566 (2013).
3. Mahmoud A.D., Lewis S., Juricic L., Udoh U.A., Hartmann S., Jansen M.A., Ogunbayo O.A., Puggioni P., Holmes A.P., Kumar P., Navarro-Dorado J., Foretz M., Viollet B., Dutia M.B., Marshall I. & Evans A.M. AMPK Deficiency Blocks the Hypoxic Ventilatory Response and Thus Precipitates Hypoventilation and Apnea. *Am. J. Respir. Crit. Care Med.* **193**, 1032-1043 (2016).
4. Wilson R.J. & Teppema L.J. Integration of Central and Peripheral Respiratory Chemoreflexes. *Compr. Physiol.* **6**, 1005-1041 (2016).
5. Teppema L.J. & Dahan A. The ventilatory response to hypoxia in mammals: mechanisms, measurement, and analysis. *Physiol. Rev.* **90**, 675-754 (2010).
6. Guyenet P.G. Neural structures that mediate sympathoexcitation during hypoxia. *Resp. Physiol.* **121**, 147-162 (2000).
7. Smith J.C., Abdala A.P., Borgmann A., Rybak I.A. & Paton J.F. Brainstem respiratory networks: building blocks and microcircuits. *Trends. Neurosci.* **36**, 152-162 (2013).
8. Nurse C.A. Synaptic and paracrine mechanisms at carotid body arterial chemoreceptors. *J. Physiol.* **592**, 3419-3426 (2014).
9. Sakamoto K., McCarthy A., Smith D., Green K.A., Hardie D.G., Ashworth A. & Alessi D.R. Deficiency of LKB1 in skeletal muscle prevents AMPK activation and glucose uptake during contraction. *EMBO J.* **24**, 1810-1820 (2005).
10. Lantier L., Fentz J., Mounier R., Leclerc J., Treebak J.T., Pehmoller C., Sanz N., Sakakibara I., Saint-Amand E., Rimbaud S., Maire P., Marette A., Ventura-Clapier R., Ferry A., Wojtaszewski

569 J.F., Foretz M. & Viollet B. AMPK controls exercise endurance, mitochondrial oxidative capacity,
570 and skeletal muscle integrity. *FASEB J,* **28**, 3211-3224 (2014).
571 11. Hirooka Y., Polson J.W., Potts P.D. & Dampney R.A. Hypoxia-induced Fos expression in
572 neurons projecting to the pressor region in the rostral ventrolateral medulla. *Neuroscience* **80**,
573 1209-1224 (1997).
574 12. Lindeberg J., Usoskin D., Bengtsson H., Gustafsson A., Kylberg A., Soderstrom S. &
575 Ebendal T. Transgenic expression of Cre recombinase from the tyrosine hydroxylase locus.
576 *Genesis* **40**, 67-73 (2004).
577 13. Anderson K.A., Ribar T.J., Lin F., Noeldner P.K., Green M.F., Muehlbauer M.J., Witters
578 L.A., Kemp B.E. & Means A.R. Hypothalamic CaMKK2 contributes to the regulation of energy
579 balance. *Cell Metab.* **7**, 377-388 (2008).
580 14. Mahmoud A.D., Lewis S., Juricic L., Udoh U.A., Hartmann S., Jansen M.A., Ogunbayo
581 O.A., Puggioni P., Holmes A.P., Kumar P., Navarro-Dorado J., Foretz M., Viollet B., Dutia M.B.,
582 Marshall I. & Evans A.M. AMP-activated Protein Kinase Deficiency Blocks the Hypoxic
583 Ventilatory Response and Thus Precipitates Hypoventilation and Apnea. *Am. J. Respir. Crit. Care*
584 *Med.* **193**, 1032-1043 (2016).
585 15. Day T.A. & Wilson R.J. Brainstem PCO2 modulates phrenic responses to specific carotid
586 body hypoxia in an in situ dual perfused rat preparation. *J. Physiol.* **578**, 843-857 (2007).
587 16. Smith C.A., Engwall M.J., Dempsey J.A. & Bisgard G.E. Effects of specific carotid body
588 and brain hypoxia on respiratory muscle control in the awake goat. *J. Physiol.* **460**, 623-640 (1993).
589 17. Curran A.K., Rodman J.R., Eastwood P.R., Henderson K.S., Dempsey J.A. & Smith C.A.
590 Ventilatory responses to specific CNS hypoxia in sleeping dogs. *J. Appl. Physiol.* **88**, 1840-1852
591 (2000).
592 18. Chapman R.W., Santiago T.V. & Edelman N.H. Effects of graded reduction of brain blood
593 flow on ventilation in unanesthetized goats. *J. Appl. Physiol. Respir. Environ. Exerc. Physiol.* **47**,
594 104-111 (1979:).
595 19. Martin-Body R.L., Robson G.J. & Sinclair J.D. Restoration of hypoxic respiratory
596 responses in the awake rat after carotid body denervation by sinus nerve section. *J. Physiol.* **380**,
597 61-73 (1986).
598 20. Hodson E.J., Nicholls L.G., Turner P.J., Llyr R., Fielding J.W., Douglas G., Ratnayaka I.,
599 Robbins P.A., Pugh C.W., Buckler K.J., Ratcliffe P.J. & Bishop T. Regulation of ventilatory
600 sensitivity and carotid body proliferation in hypoxia by the PHD2/HIF-2 pathway. *J. Physiol.* **594**,
601 1179-1195 (2016).
602 21. Martin-Body R.L., Robson G.J. & Sinclair J.D. Respiratory effects of sectioning the carotid
603 sinus glossopharyngeal and abdominal vagal nerves in the awake rat. *J Physiol* **1361**, 35-45 (1985).
604 22. Li P., Janczewski W.A., Yackle K., Kam K., Pagliardini S., Krasnow M.A. & Feldman J.L.
605 The peptidergic control circuit for sighing. *Nature* **530**, 293-297 (2016).
606 23. Ross F.A., Rafferty J.N., Dallas M.L., Ogunbayo O., Ikematsu N., McClafferty H., Tian L.,
607 Widmer H., Rowe I.C., Wyatt C.N., Shipston M.J., Peers C., Hardie D.G. & Evans A.M. Selective
608 Expression in Carotid Body Type I Cells of a Single Splice Variant of the Large Conductance
609 Calcium- and Voltage-activated Potassium Channel Confers Regulation by AMP-activated Protein
610 Kinase. *J. Biol. Chem.* **286**, 11929-11936 (2011).
611 24. Blain G.M., Smith C.A., Henderson K.S. & Dempsey J.A. Peripheral chemoreceptors
612 determine the respiratory sensitivity of central chemoreceptors to CO(2). *J Physiol* **588**, 2455-2471
613 (2010).

614 25. Ponikowski P., Chua T.P., Anker S.D., Francis D.P., Doehner W., Banasiak W., Poole-
615 Wilson P.A., Piepoli M.F. & Coats A.J. Peripheral chemoreceptor hypersensitivity: an ominous
616 sign in patients with chronic heart failure. *Circulation* **104**, 544-549 (2001).
617 26. Hall M.J., Xie A., Rutherford R., Ando S., Floras J.S. & Bradley T.D. Cycle length of
618 periodic breathing in patients with and without heart failure. *Am. J. Respir. Crit. Care Med.* **154**,
619 376-381 (1996).
620 27. Topor Z.L., Vasilakos K., Younes M. & Remmers J.E. Model based analysis of sleep
621 disordered breathing in congestive heart failure. *Resp. Physiol. Neurobiol.* **155**, 82-92 (2007).
622 28. Bell H.J. & Azubike E, Haouzi P. The "other" respiratory effect of opioids: suppression of
623 spontaneous augmented ("sigh") breaths. *J. Appl. Physiol.* **111**, 1296-1303 (2011).
624 29. Wade J.G., Larson C.P. Jr., Hickey R.F., Ehrenfeld W.K. & Severinghaus J.W. Effect of
625 carotid endarterectomy on carotid chemoreceptor and baroreceptor function in man. *New England*
626 *J. Med.* **282**, 823-829 (1970).
627 30. Pascual O., Morin-Surun M.P., Barna B., Denavit-Saubie M., Pequignot J.M. &
628 Champagnat J. Progesterone reverses the neuronal responses to hypoxia in rat nucleus tractus
629 solitarius in vitro. *J. Physiol.* **544**, 511-520 (2002).
630 31. Nolan P.C. & Waldrop T.G. In vivo and in vitro responses of neurons in the ventrolateral
631 medulla to hypoxia. *Brain Res.* **630**, 101-114 (1993).
632 32. Sun M.K. & Reis D.J. Differential responses of barosensitive neurons of rostral
633 ventrolateral medulla to hypoxia in rats. *Brain Res.* **609**, 333-337 (1993).
634 33. Angelova P.R., Kasymov V., Christie I., Sheikhbahaei S., Turovsky E., Marina N., Korsak
635 A., Zwicker J., Teschemacher A.G., Ackland G.L., Funk G.D., Kasparov S., Abramov A.Y. &
636 Gourine A.V. Functional Oxygen Sensitivity of Astrocytes. *J. Neurosci.* **35**, 10460-10473 (2015).
637 34. Magistretti P.J. & Allaman I. Lactate in the brain: from metabolic end-product to signalling
638 molecule. *Nat. Rev. Neurosci.* **19**, 235-249 (2018).
639 35. Roux J.C. & Villard L. Biogenic amines in Rett syndrome: the usual suspects. *Behavior*
640 *Genetics* **40**, 59-75 (2010).
641 36. Mulligan E. & Lahiri S. Separation of carotid body chemoreceptor responses to O2 and
642 CO2 by oligomycin and by antimycin A. *Am. J. Physiol.* **242**, C200-206 (1982).
643 37. Dasso L.L., Buckler K.J., Vaughan-Jones R.D. Interactions between hypoxia and
644 hypercapnic acidosis on calcium signaling in carotid body type I cells. *Am. J. Physiol.* **279**, L36-
645 42 (2000).
646 38. Pepper D.R., Landauer R.C. & Kumar P. Postnatal development of CO2-O2 interaction in
647 the rat carotid body in vitro. *J. Physiol.* **485**, 531-541 (1995).
648 39. Murali S. & Nurse C.A. Purinergic signalling mediates bidirectional crosstalk between
649 chemoreceptor type I and glial-like type II cells of the rat carotid body. *J. Physiol.* **594**, 391-406
650 (2016).
651 40. Shaw R.J., Lamia K.A., Vasquez D., Koo S.H., Bardeesy N., Depinho R.A., Montminy M.
652 & Cantley L.C. The kinase LKB1 mediates glucose homeostasis in liver and therapeutic effects of
653 metformin. *Science* **310**, 1642-1646 (2005).
654 41. Patel K., Foretz M., Marion A., Campbell D.G., Gourlay R., Boudaba N., Tournier E.,
655 Titchenell P., Peggie M., Deak M., Wan M., Kaestner K.H., Goransson O., Viollet B., Gray N.S.,
656 Birnbaum M.J., Sutherland C. & Sakamoto K. The LKB1-salt-inducible kinase pathway functions
657 as a key gluconeogenic suppressor in the liver. *Nature Comm.* **5**, 4535 (2014).
658 42. Gan B., Hu J., Jiang S., Liu Y., Sahin E., Zhuang L., Fletcher-Sananikone E., Colla S.,
659 Wang Y.A., Chin L., Depinho R.A. Lkb1 regulates quiescence and metabolic homeostasis of
660 haematopoietic stem cells. *Nature* **468**, 701-704 (2010).

661 43. Swisa A., Granot Z., Tamarina N., Sayers S., Bardeesy N., Philipson L., Hodson D.J.,
662 Wikstrom J.D., Rutter G.A., Leibowitz G., Glaser B. & Dor Y. Loss of Liver Kinase B1 (LKB1)
663 in Beta Cells Enhances Glucose-stimulated Insulin Secretion Despite Profound Mitochondrial
664 Defects. *J. Biol. Chem.* **290**, 20934-20946 (2015).
665 44. Lizcano J.M., Goransson O., Toth R., Deak M., Morrice N.A., Boudeau J., Hawley S.A.,
666 Udd L., Makela T.P., Hardie D.G., Alessi D.R. LKB1 is a master kinase that activates 13 kinases
667 of the AMPK subfamily, including MARK/PAR-1. *EMBO J.* **23**, 833-843 (2004).
668 45. Ikematsu N., Dallas M.L., Ross F.A., Lewis R.W., Rafferty J.N., David J.A., Suman R.,
669 Peers C., Hardie D.G. & Evans A.M. Phosphorylation of the voltage-gated potassium channel
670 Kv2.1 by AMP-activated protein kinase regulates membrane excitability. *PNAS* **108**, 18132-18137
671 (2011).
672 46. Lipton A.J., Johnson M.A., Macdonald T., Lieberman M.W., Gozal D. & Gaston B. S-
673 nitrosothiols signal the ventilatory response to hypoxia. *Nature* **413**, 171-174 (2001).
674 47. Murphy B.A., Fakira K.A., Song Z., Beuve A., Routh V.H. AMP-activated protein kinase
675 and nitric oxide regulate the glucose sensitivity of ventromedial hypothalamic glucose-inhibited
676 neurons. *Am. J. Physiol.* **297**, C750-758 (2009).
677 48. Chau E.H., Lam D., Wong J., Mokhlesi B. & Chung F. Obesity hypoventilation syndrome:
678 a review of epidemiology, pathophysiology, and perioperative considerations. *Anesthesiology* **117**,
679 188-205 (2012).
680 49. Ainslie P.N., Lucas S.J. & Burgess K.R. Breathing and sleep at high altitude. *Respir.*
681 *Physiol. Neurobiol.* **188**, 233-256 (2013).
682 50. Wyatt C.N., Mustard K.J., Pearson S.A., Dallas M.L., Atkinson L., Kumar P., Peers C.,
683 Hardie D.G. & Evans A.M. AMP-activated protein kinase mediates carotid body excitation by
684 hypoxia. *J. Biol. Chem.* **282**, 8092-8098 (2007).
685 51. Holmes A.P., Turner P.J., Buckler K.J. & Kumar P. Moderate inhibition of mitochondrial
686 function augments carotid body hypoxic sensitivity. *Pflugers Arch.* **468**, 143-155 (2016).
687 52. Vidruk E.H., Olson E.B. Jr., Ling L. & Mitchell G.S. Responses of single-unit carotid body
688 chemoreceptors in adult rats. *J. Physiol.* **531**, 165-170 (2001).
689

690

FIGURES AND LEGENDS

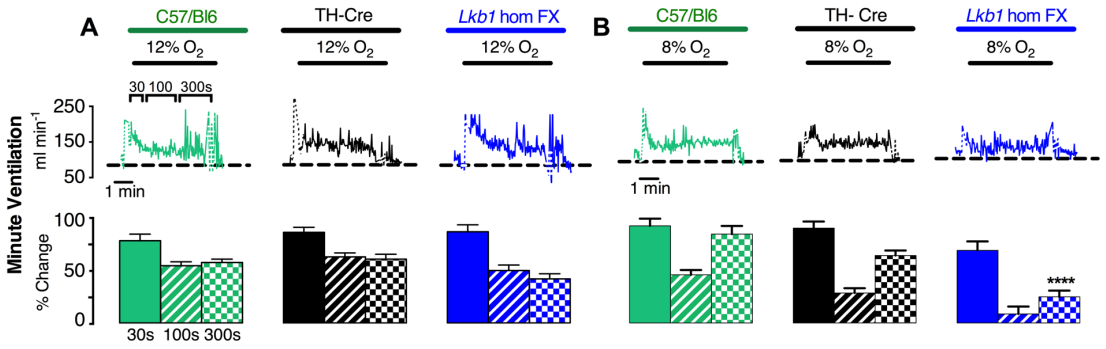

Figure 1 - Mice hypomorphic for Lkb1 exhibit an attenuated hypoxic ventilatory response measured by unrestrained plethysmography.

Upper panels show example records and *lower panels* bar charts of mean±SEM for increases in minute ventilation at the peak of the Augmenting Phase (A, ~30s), after Roll Off (RO, ~100s) and during the plateau of the Sustained Phase (SP, ~300s) of the ventilatory response to (*A*) 12% and (*B*) 8% O_2 for C57Bl6 (green, n = 6), TH-Cre (black, n = 31) and *Lkb1* homozygous floxed mice (*Lkb1* hom FX, blue, n = 14) which are globally hypomorphic (~90% loss of Lkb1). ****=p< 0.0001 relative to TH-Cre and C57/Bl6.

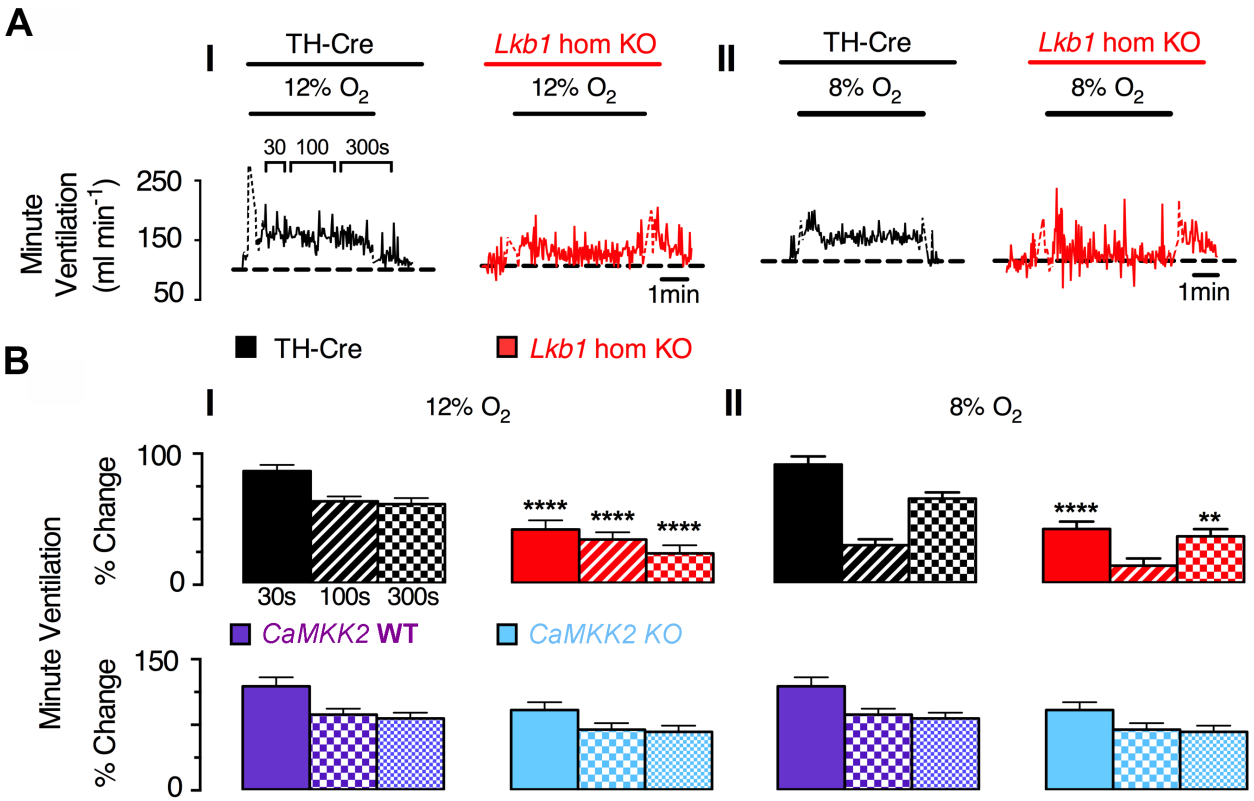

Figure 2 - Conditional deletion of *Lkb1* in tyrosine hydroxylase expressing cells markedly attenuates the hypoxic ventilatory response measured by unrestrained plethysmography, but global *CaMKK2* knockout does not.

A, Example records of minute ventilation (ml min^{-1} g^{-1}) versus time during (I) 12% O_2 and (II) 8% O_2 for TH-Cre (black, n = 31) and conditional *Lkb1* knockout mice (*Lkb1* hom KO, red, n = 22). B, Bar charts show mean±SEM for changes in minute ventilation at the peak of the Augmenting Phase (A, ~30s), at 100s following Roll Off (RO, ~100s) and the plateau of the Sustained Phase (SP, 300s) of the response to hypoxia of (*Upper Panels*) TH-Cre (black, n = 31) conditional *Lkb1* hom KO (red, n = 22) and (*Lower Panels*) *CaMKk2 WT* (purple, n = 7) and global *CaMKK2* KO (blue, n = 7). *=p<0.05, **** = p < 0.00001.

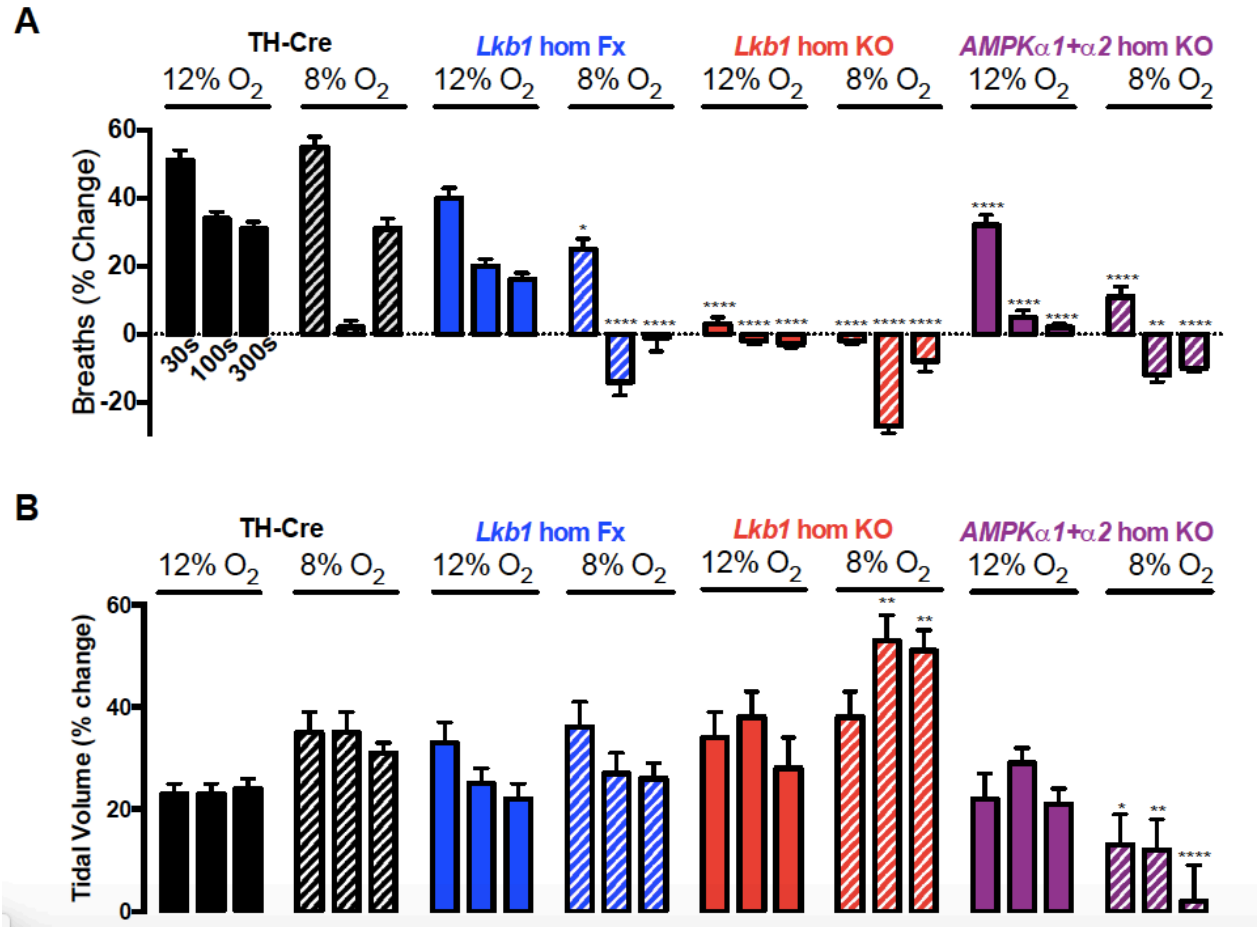

Figure 3 - Conditional deletion of *Lkb1* in tyrosine hydroxylase expressing cells blocks increases in breathing frequency but augments increases in tidal volume during severe hypoxia measured by unrestrained plethysmography.

Bar charts of mean±SEM for increases in (A) Breathing frequency and (B) Tidal volume At the peak of the Augmenting Phase (~30s), at ~100s following Roll Off and during the plateau of the Sustained Phase (~300s) of the ventilatory response to hypoxia for TH-Cre (black, n = 31), *Lkb1* homozygous floxed mice (*Lkb1* hom Fx, blue, n = 22) that are ~90% hypomorphic for Lkb1 and conditional *Lkb1* homozygous knockout mice (*Lkb1* hom KO, red, n = 22). These data are also compared with outcomes for conditional *AMPKα1+α2* homozygous knockout mice (*AMPKα1+α2* hom KO, mauve, n = 26-30). *=p<0.05, **=p<0.01, ****=p< 0.0001 compared to TH-Cre.

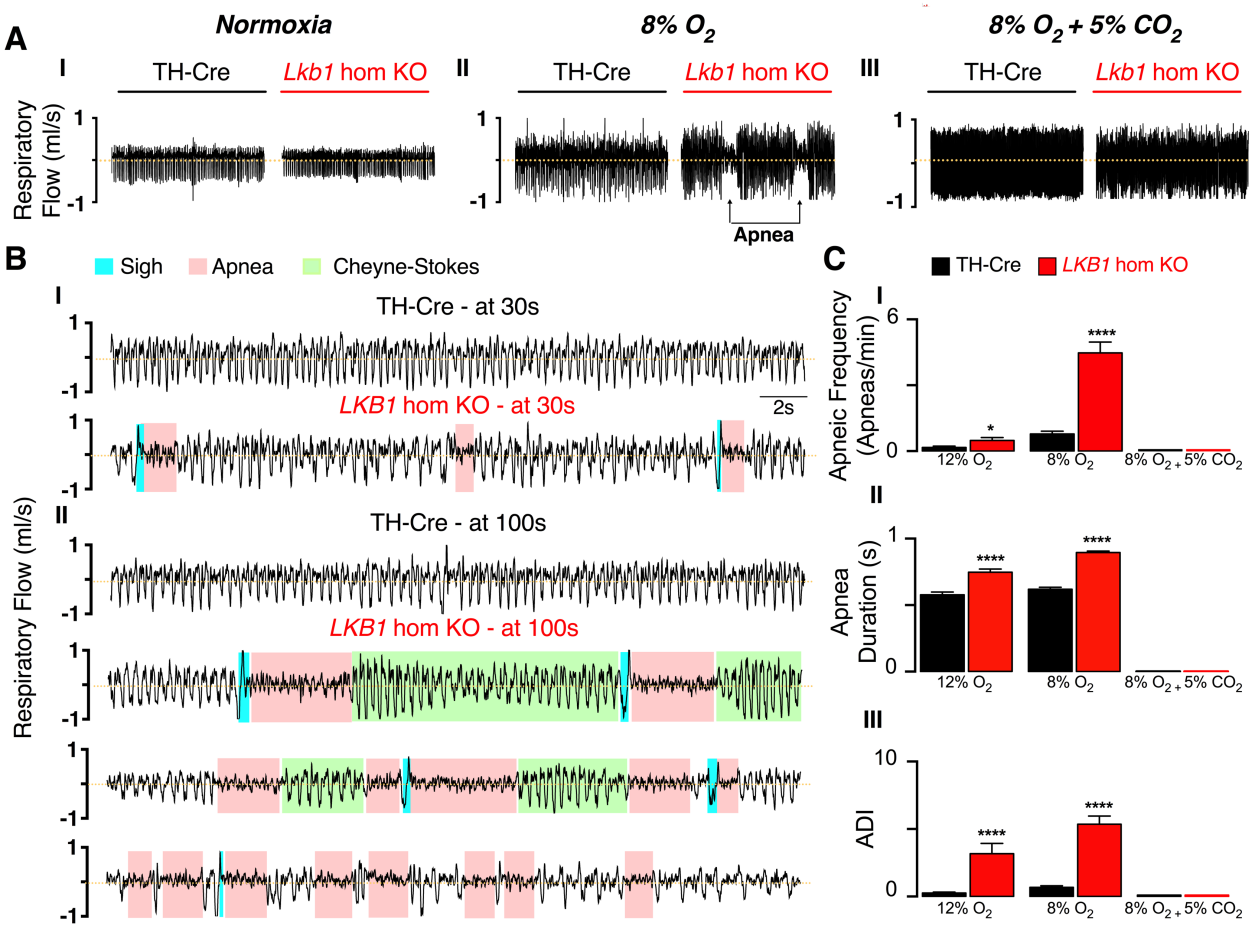

Figure 4 - Unrestrained plethysmography shows that conditional deletion of *Lkb1* in tyrosine hydroxylase expressing cells precipitates hypoventilation, apnoea and Cheyne-Stokes-like breathing during severe hypoxia.

A, Example records of ventilatory activity from TH-Cre and conditional *Lkb1* homozygous knockout mice (*Lkb1* hom KO) during (*I*) normoxia (21% O_2), (*II*) hypoxia (8% O_2) and (*III*) hypoxia with hypercapnia (8% O_2 + 5% CO_2), that were obtained using whole body plethysmography. B(I-II), Typical ventilatory records for TH-Cre and conditional *Lkb1* hom KO mice on an expanded time scale at the indicated time points during exposures to severe hypoxia (8% O_2). C, mean±SEM for (*I*) apnoeic index (per minute), (*II*) apnoea duration (s) and (*III*) apnoea-duration index (frequency x duration) for TH-Cre (black, n = 31) and conditional *Lkb1* hom KO (red, n = 22) mice during exposures to 12% O_2, 8% O_2 and 8% O_2 + 5% CO_2. *=p<0.05, ****=p< 0.0001.

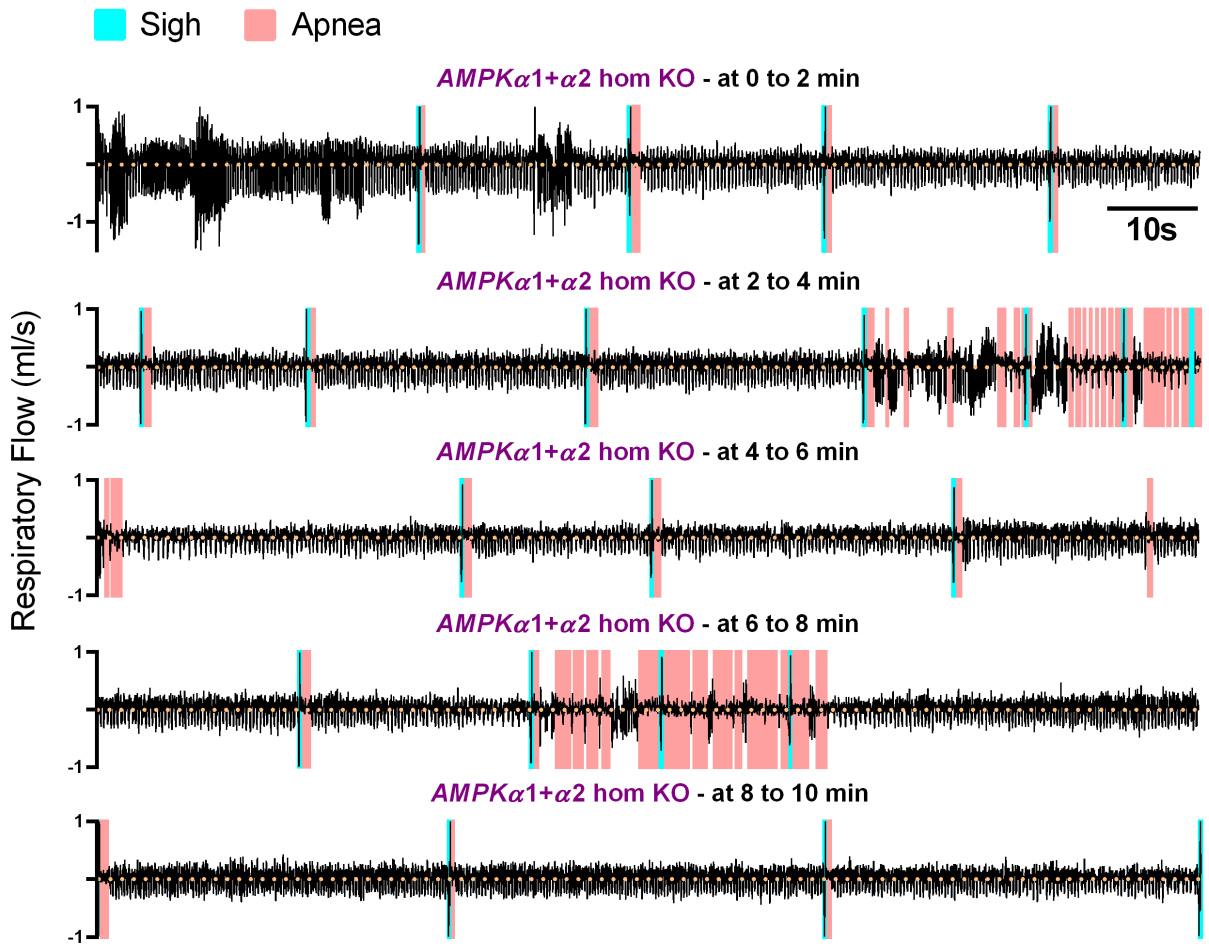

Figure 5 - Conditional deletion of *AMPK-α1+α2* in tyrosine hydroxylase expressing cells does not precipitate Cheyne-Stokes-like ventilation even during prolonged 10 minute exposures to severe hypoxia during unrestrained plethysmography.
Typical ventilatory record for conditional *AMPK-α1+α2* double knockout mice (*AMPKα1+α2* hom KO) during a 10 minute exposure to severe hypoxia (8% O_2).

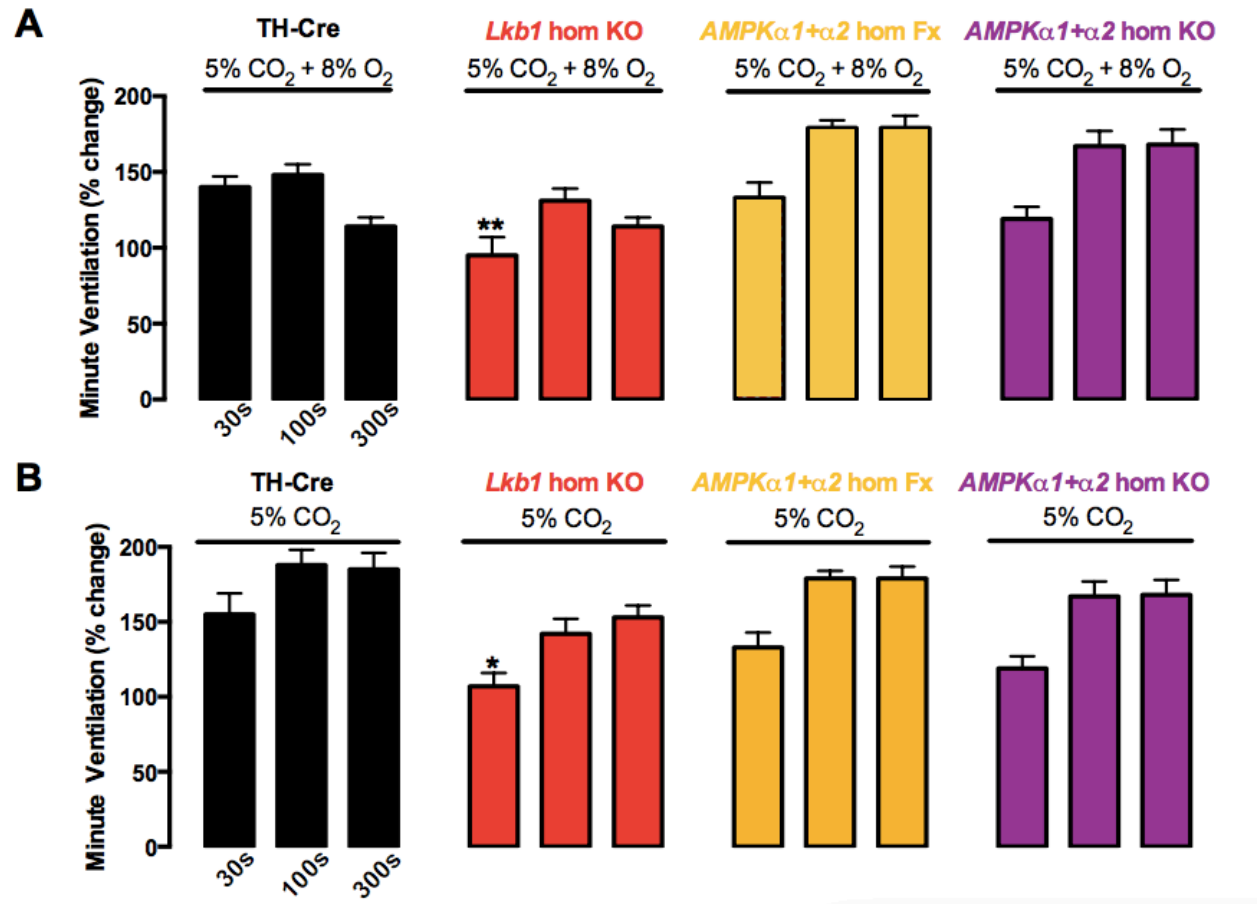

Figure 6 - Conditional deletion of Lkb1 in tyrosine hydroxylase expressing cells markedly slows the hypercapnic ventilatory response measured by unrestrained plethysmography. Bar charts of mean±SEM for increases in minute ventilation at ~30s, 100s and 300s during exposures to (A) Hypercapnic hypoxia (5% CO_2+8%O2) and (B) Hypercapnia (5% CO_2) for TH-Cre (black, n = 31), conditional *Lkb1* homozygous knockout mice (*Lkb1* hom KO, red, n = 22), *AMPKα1+α2* homozygous floxed mice (*AMPKα1+α2* hom Fx, beige, n = 26) and *AMPKα1+α2* homozygous knockout mice (*AMPKα1+α2* hom KO, mauve, n = 30). *=p<0.05, **=p< 0.0001.

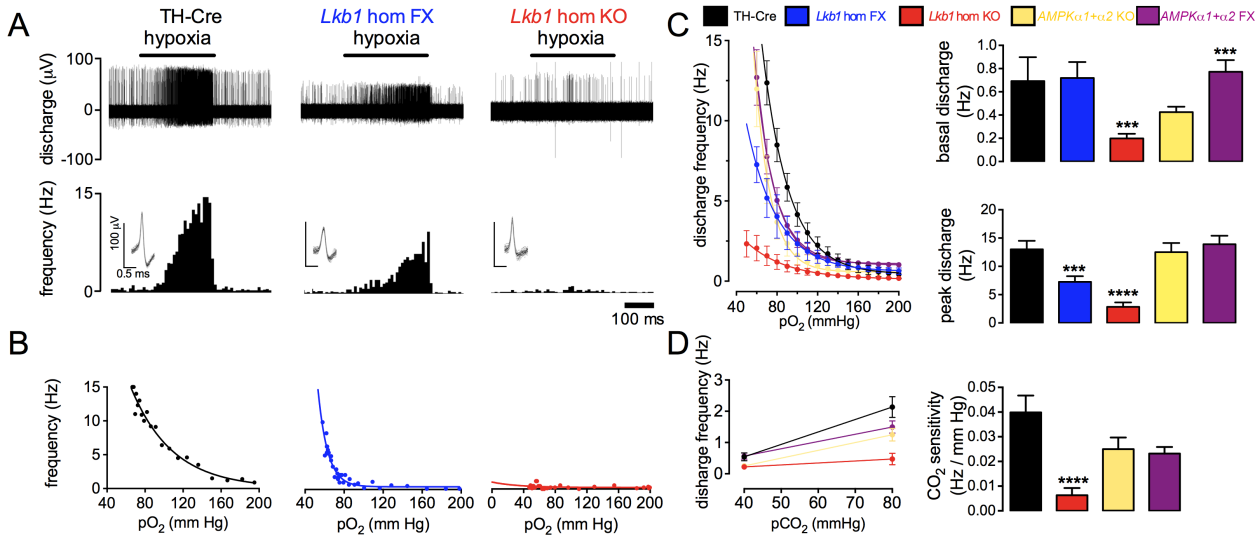

Figure 7 – Conditional deletion of *Lkb1* but not *AMPK-α1*+α2 in tyrosine hydroxylase positive cells attenuates afferent discharge from the carotid body in-vitro during normoxia, hypoxia and hypercapnia

A, *Upper panels* show extracellular recordings of chemoafferent discharge versus time for carotid bodies from control (TH-Cre, black), *Lkb1* homozygoous floxed (*Lkb1* hom FX, blue) and conditional *Lkb1* homozygous knockout (*Lkb1* hom KO, red) mice*, Lower panels* show frequency-time histograms (*inset:* single fibre discriminations). B, Frequency-pO_2 response curves corresponding to records in (*A*). C, *Left hand panel* compares mean±SEM for frequency-pO_2 response curves for TH-Cre (black, n = 8), *Lkb1* hom FX (blue, n = 7), conditional *Lkb1* hom KO (red, n = 7), *AMPK-α1* and -α2 double floxed *(AMPK* hom FX, beige, n=5) and conditional *AMPK-α1*+α2 double knockouts (*AMPK* hom DKO, mauve, n=5). Bar charts in *right hand panels* show mean±SEM for (*upper*) basal single fibre discharge frequency and (*lower*) peak single fibre discharge frequency during hypoxia. D, Mean±SEM for chemoafferent discharge versus pCO_2 (*left hand panel*) and CO_2 sensitivity (*right hand panel*) for TH-Cre, *Lkb1* hom KO, *AMPK* hom FX *and AMPK* hom DKO. *** =p<0.001, ****=p< 0.0001.

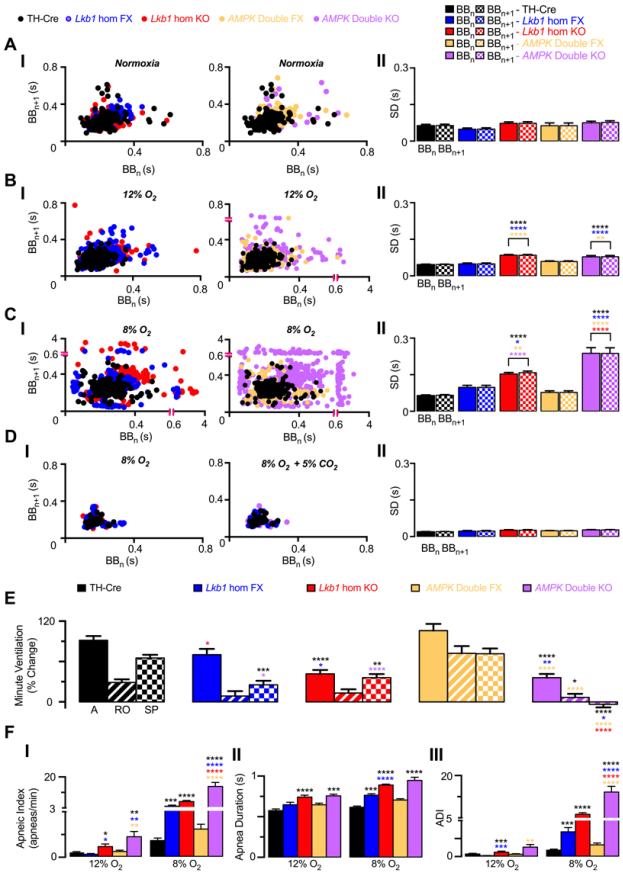

Figure 8 – Unrestrained plethysmography reveals that respiratory dysfunction during hypoxia is less severe for conditional *Lkb1* deletion than for conditional *AMPK-α1+α2* deletion in catecholaminergic cells.

AI, *Lefthand panel* shows exemplar Poincaré plots of the inter-breath interval (BB_n) versus subsequent interval (BB_{n+1}) during normoxia for controls (TH-Cre, black, n=31), *Lkb1 homozygous* floxed (*Lkb1* hom FX, blue, n=14) and conditional *Lkb1* homozygous knockouts (*Lkb1* hom KO, red, n=22). *Right hand panel* shows comparable data for *AMPK-α1+α2* double floxed mice (*AMPK* hom FX, n=31) and conditional *AMPK-α1+α2* double knockouts (*AMPK* hom DKO, n=22). AII, Corresponding mean±SEM for the standard deviation (SD) of BB_n and BB_{n+1} for each genotype are shown for normoxia. BI, Poincaré plots of BB_n versus BB_{n+1} for mild hypoxia (12% O_2). BII, Corresponding mean±SEM for the standard deviation (SD) of BB_n and BB_{n+1} for each genotype are shown for mild hypoxia (12% O_2). CI, Poincaré plots of BB_n versus BB_{n+1} for severe hypoxia (8% O_2). CII, Corresponding mean±SEM for the standard deviation (SD) of BB_n and BB_{n+1} for each genotype are shown for severe hypoxia (8% O_2). DI, Poincaré plots of BB_n versus BB_{n+1} for hypercapnic hypoxia (8% O_2 + 5% CO_2). Corresponding mean±SEM for the standard deviation (SD) of BB_n and BB_{n+1} for each genotype are shown for hypercapnic hypoxia (8% O_2 + 5% CO_2). E, Comparison for all genotypes tested of mean±SEM for the % change of minute ventilation at the peak of the Augmenting Phase (~30s), at ~100s following Roll Off and during the plateau of the Sustained Phase (~300s) during exposures to 8% O_2. F, Comparison for all genotypes tested of the mean±SEM for (*I*) apnoeic index (per minute), (*II*) apnoea duration (s) and (*III*) apnoea-duration index (frequency x duration).

*=p<0.05, **=p<0.01, *** =P<0.001, ****=p< 0.0001.